Proceedings of the Thirty-fourth (2024) International Ocean and Polar Engineering Conference **www.isope.org**
Rhodes, Greece, June 16–21, 2024

ISBN 978-1-880653-78-4; ISSN 1098-6189

Three-dimensional Simulations of Tsunamis Induced by Rigid Landslide by Resolved MPS-DEM Method

*Fengze Xie[1], Jifei Wang[2], Decheng Wan[1]**

[1] Computational Marine Hydrodynamics Lab (CMHL), School of Naval Architecture, Ocean and Civil Engineering, Shanghai Jiao Tong University, Shanghai, China
[2] Shanghai Aerospace System Engineering Institute, Shanghai, China

*Corresponding author

ABSTRACT

In this paper, a 3-D resolved MPS-DEM solver is developed for the simulation of tsunamis induced by rigid landslide. The fluid-slide-ramp interaction model is established based on the collision model and Pressure Integration (PI) method. In order to avoid the simultaneous participation of adjacent boundary particles of rigid slide and ramp in solving Pressure Poisson Equation (PPE) solution, a Dynamic Boundary particle Labeling (DBL) technique is proposed. Then, this solver is applied to simulate the subaerial and rigid landslide. Numerical results are in good agreement with experimental data.

KEY WORDS: MPS-DEM resolved method; Pressure integration; Dynamic boundary particle labeling; Rigid landslides.

INTRODUCTION

Due to changes of ocean environmental loads, surges induced by rigid landslides often occur. During the process of rigid landslides, the rigid landslide is simultaneously subjected to forces imposed by the ramp and fluid. And the nonlinear waves are generated and propagated. The waves may damage coastal marine engineering facilities and ships docked or sailing near the shore, and even threaten human life safety. However, due to the complex hydrodynamic pressure, it is difficult to accurately predict the trajectory of the landslide and the time histories of wave height. Therefore, how to predict the process of rigid landslide and the resulting wave propagation is always a difficult problem in coastal engineering research, which deserves the attention of researchers.

With the rapid development of computer hardware, Computer Aided Engineering (CAE) technology has been developed continuously. For the simulation of fluid, Computational Fluid Dynamics (CFD) methods can be classified as mesh-based method and particle-based methods. There are no complex topological relationships between particles. Therefore, particle-based methods, such as Smoothed Particle Hydrodynamics (SPH) method and Moving Particle Semi-implicit (MPS) method, are better at capturing large deformations of free surfaces. Besides, the slide with arbitrary shape can be discretized into particles (Ji et al., 2020; Zhu et al., 2021; Peng et al., 2021). By establishing a six-degree-of-freedom model, the interaction between the floating body and the fluid can be simulated. Discrete Element Method (DEM), as a mature solid mechanics calculation method, is often used to simulate the interaction between solids. By arranging DEM particles on the surface of a solid body, a solid-solid interaction model can be further built.

In traditional strategies, the movement trajectory and velocity of the rigid slide are given before numerical simulation. However, the influence of fluid on the rigid slide is ignored. In addition, without experimental results, it is difficult to use those methods to study the fluid-rigid slide interaction process in other cases. Therefore, how to correctly simulate the interaction between contact surfaces is also a key concern for scholars. Amicarelli et al. (2015) proposed a SPH-based model that can simulate low-velocity collisions between solids. Yeylaghi et al. (2017) arranged a layer of Interface Fluid Particles (IFP) between the slide and the ramp. The IFP have the same properties and governing equations as fluid particles. However, the information of velocity and displacement of the IFP is given by the landslide particles. Zhang et al. (2021) proposed a motion model based on the formula of sliding friction. Wang et al. (2016) used the Discontinuous Deformation Analysis (DDA) method to simulate the movement of the rigid landslide. hydrodynamic load calculated by SPH is transferred to DDA, which provides dynamic boundary information for SPH. Tan et al. (2018) simulated the surge induced by rigid landslide using the SPH-DEM coupling method. Empirical formula is used to calculate the hydrodynamics exerted to the rigid landslide. Xu et al. (2021) proposed a SPH-DEM coupling method. The SPH ghost particles and DEM particles serve as the boundary of the rigid landslide. The reaction force of the boundary ghost particles on the fluid particles is the hydrodynamic force applied on the rigid slide. The boundary ghost particles move with DEM slide. In the above methods, the fluid forces or contact forces applied on the rigid landslide are mostly simplified. Therefore, it is necessary to establish a more accurate fluid-rigid slide-ramp interaction model.

The numerical methods have been widely used to investigated waves induced by the rigid landslide. Heller et al. (2016) used physical experiments and an open-source software (DualSPHysics) based on the SPH method to study the surge phenomenon caused by the landslide of

a solid with the leading-edge angle of 45°. 2-D landslides and 3-D landslides were compared in detail. Tan et al. (2018) compared the waves caused by rigid and granular slide based on the SPH-DEM method and studied the energy exchange and during the landslide process. Yeylaghi et al. (2017) used experiments and the ISPH method to study the interaction between the slide and non-Newtonian fluid (water-bentonite mixture). The experimental results of the free surface height variation are very close to the numerical results. Qi et al. (2022) simulated the waves induced by multi-block landslide based on the SPH method. They demonstrated the complexity of waves with energy analysis.

In this work, a 3-D resolved MPS-DEM solver for the simulation of landslides is developed. Firstly, the improved MPS method, the DEM method and MPS-DEM coupled strategy are presented briefly. Then, two cases, including the subaerial landslide and submerged landslide, are simulated and compared with experimental data to validate the 3-D solver.

NUMERICAL METHOD

MPS formulation for fluid dynamics

The fluid governing equations, including the continuity equation and momentum equation, can be written as follows:

$$\frac{D\rho_f}{Dt} + \rho_f \nabla \cdot \boldsymbol{u}_f = 0 \tag{1}$$

$$\rho_f \frac{D\boldsymbol{u}_f}{Dt} = -\nabla p + \mu_f \nabla^2 \boldsymbol{u}_f + \rho_f \boldsymbol{g} \tag{2}$$

where subscript f represents fluid, $\boldsymbol{u}_f$ is fluid velocity vector, ρ_f is fluid density, t is physical time, ∇ represents the Hamiltonian operator, p represents fluid pressure, μ_f is the dynamic viscosity coefficient of the fluid, $\boldsymbol{g}$ is the acceleration vector of gravity.

The interaction between MPS particles is controlled by the Kernel Function (KF). A KF proposed by Zhang et al. (2014) is adopted in this paper, which is written as follows:

$$w(r) = \begin{cases} \dfrac{r_e}{0.85r + 0.15r_e} - 1 & 0 \le r < r_e \\ 0 & r \ge r_e \end{cases} \tag{3}$$

where r represents the distance between MPS neighbor particles, r_e represents the effective radius.

The inter-particle interaction models including the gradient model, divergence model, and Laplacian model are written as,

$$\langle \nabla \phi \rangle_i = \frac{d}{n^0} \sum_{j \ne i} \frac{\phi_j + \phi_i}{|\boldsymbol{r}_j - \boldsymbol{r}_i|^2} (\boldsymbol{r}_j - \boldsymbol{r}_i) w(|\boldsymbol{r}_j - \boldsymbol{r}_i|) \tag{4}$$

$$\langle \nabla \cdot \boldsymbol{\Phi} \rangle_i = \frac{d}{n^0} \sum_{j \ne i} \frac{(\boldsymbol{\Phi}_j - \boldsymbol{\Phi}_i) \cdot (\boldsymbol{r}_j - \boldsymbol{r}_i)}{|\boldsymbol{r}_j - \boldsymbol{r}_i|^2} w(|\boldsymbol{r}_j - \boldsymbol{r}_i|) \tag{5}$$

$$\langle \nabla^2 \phi \rangle_i = \frac{2d}{n^0 \lambda} \sum_{j \ne i} (\phi_j - \phi_i) w(|\boldsymbol{r}_j - \boldsymbol{r}_i|) \tag{6}$$

where subscripts i and j represent the number of fluid particles, $\boldsymbol{r}_i$ and $\boldsymbol{r}_j$ are the position vectors of fluid particles i and j, ϕ is the physical scalar carried by the MPS particles, $\boldsymbol{\Phi}$ represents the physical vector carried by the MPS particles, d is the spatial dimension of the computational domain, n^0 is the particle number density under the initial distribution, λ is a correction parameter, which is a compensation for the error caused by using a finite range kernel function to approximate an infinite range Gaussian function in the derivation process of the Laplace model, written as,

$$\lambda = \frac{\sum_{j \ne i} w(|\boldsymbol{r}_j - \boldsymbol{r}_i|) |\boldsymbol{r}_j - \boldsymbol{r}_i|^2}{\sum_{j \ne i} w(|\boldsymbol{r}_j - \boldsymbol{r}_i|)} \tag{7}$$

Pressure information is obtained by solving the Pressure Poisson Equation (PPE). In order to balance between stability and accuracy, a mixed source method (Tanaka et al., 2010; Khayyer and Gotoh, 2011) is adopted, defined by,

$$\langle \nabla^2 p^{m+1} \rangle_i = (1-\gamma) \frac{\rho}{\Delta t} \nabla \cdot \boldsymbol{u}_i^* - \gamma \frac{\rho}{\Delta t^2} \frac{\langle n^m \rangle_i - n^0}{n^0} \tag{8}$$

DEM formulation for solid contact

The discrete element method was firstly proposed by Cundall and Strack (1979). The DEM particles are treated as soft spheres, and the contact force between particles is determined by the overlap size of two colliding particles. The contact model consists of three parts: springs, dampers, and sliders.

The contact force $\boldsymbol{F}_{kr}^C$ between DEM particles and ramp can be decomposed into the normal component $\boldsymbol{F}_{kr}^{C,n}$ and tangential component $\boldsymbol{F}_{kr}^{C,t}$. Both components consist of elastic force and damping force.

$$\boldsymbol{F}_{kr}^{C,n} = -\chi^n \boldsymbol{\delta}_{kr}^n - \eta^n \boldsymbol{v}_{kr}^n \tag{11}$$

$$\boldsymbol{F}_{kr}^{C,t} = \begin{cases} -\chi^t \boldsymbol{\delta}_{kr}^t - \eta^t \boldsymbol{v}_{kr}^t & |\boldsymbol{F}_{kr}^{C,t}| < \mu_s |\boldsymbol{F}_{kr}^{C,n}| \\ -\mu_s |\boldsymbol{F}_{kr}^{C,n}| \dfrac{\boldsymbol{\delta}_{kr}^t}{|\boldsymbol{\delta}_{kr}^t|} & |\boldsymbol{F}_{kr}^{C,t}| > \mu_s |\boldsymbol{F}_{kr}^{C,n}| \end{cases} \tag{12}$$

where $\boldsymbol{\delta}_{kr}^n$ and $\boldsymbol{\delta}_{kr}^t$ are the normal and tangential displacement of the particle, $\boldsymbol{v}_{kr}^n$ and $\boldsymbol{v}_{kr}^t$ are the normal and tangential velocity of the particle, $\chi^n$and χ^t are the normal and tangential stiffness, η^n and η^t are the normal and tangential damping coefficient, μ_s is the friction coefficient.

MPS-DEM coupled model

DEM particles are arranged on the surface of rigid slide as shown in Fig. 1. The contact forces and contact moments between the rigid slide and the ramp can be calculated using DEM particles. The rigid slide is also regarded as a floating body, and the hydrodynamic force exerted on the sliding body is calculated by pressure integration. The governing equation for the rigid slide can be expressed as,

$$m_S \frac{d\boldsymbol{V}_S}{dt} = m_S \boldsymbol{g} + \boldsymbol{F}_S^C + \boldsymbol{F}_H^{\text{int}} \tag{13}$$

$$I_S \frac{d\boldsymbol{\omega}_S}{dt} = \boldsymbol{M}_S^C + \boldsymbol{M}_H^{\text{int}} \tag{14}$$

where m_S is the mass of the rigid slide, $\boldsymbol{V}_S$ is the velocity of the rigid slide, $\boldsymbol{F}_S^C$ is the contact force exerted on the rigid slide, $\boldsymbol{F}_H^{\text{int}}$ is the hydrodynamic force, I_S is the rotational inertia, $\boldsymbol{\omega}_S$ is the angular velocity, $\boldsymbol{M}_S^C$ is the contact moment. $\boldsymbol{M}_H^{\text{int}}$ is the moment caused by fluid dynamics.

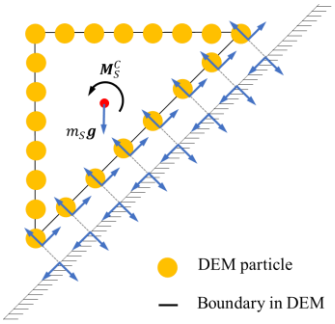

Fig. 1 Schematic diagram of rigid slide model

In MPS method, the floating body is composed of boundary particles. The wall particles of the rigid possess the characteristics of both MPS particles and DEM particles, which can be used to calculate the hydrodynamic force and contact force exerted on the rigid slide respectively. The hydrodynamic force and hydrodynamic moment acting on the rigid slide are given by,

$$\boldsymbol{F}_S^C = -\sum_i p_i \cdot \boldsymbol{n} \cdot \Delta S_i \qquad (15)$$

$$\boldsymbol{M}_H^{\text{int}} = -\sum_i \boldsymbol{r}_{G,i} \times (p_i \cdot \boldsymbol{n} \cdot \Delta S_i) \qquad (16)$$

where p_i is the hydrodynamic pressure exerted on the wall particle i in the MPS, ΔS_i is the corresponding unit area, $\boldsymbol{r}_{G,i}$ is the position vector of the wall particle relative to the center of mass of the rigid slide.

Boundary particle Labeling (DBL) technique

In the original MPS method, all wall particles that may interact with the the fluid particles participate in solving the pressure Poisson equation. In the fluid-rigid slide interaction problem, the wall particles of rigid slide and the wall particles of ramp are neighboring particles of each other, which affects the stability and accuracy of pressure field solution. Therefore, a Dynamic Boundary particle Labeling technique (DBL), as shown in Fig. 2. All wall particles are initialized as the ghost particles, and when fluid particles approach the boundary, the boundary particles are dynamically labeled as the wall particles.

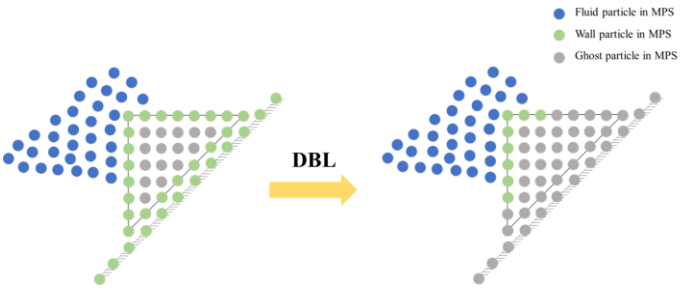

Fig. 2 Schematic diagram of Dynamic Boundary particle Labeling (DBL) technique

NUMERICAL RESULTS

Submarine rigid landslide

In this sub-section, the submarine rigid landslide is simulated and numerical results are compared with the experimental data obtained by Heinrich (1992). The test model is shown in Fig. 3. The entire experiment is conducted in a narrow water channel with width of 0.55 m, water depth of 1.0 m. The fluid density id 997 kg/m^3 and kinematic viscosity is 1.01×10^{-6} m^2/s. A rigid slide with the cross-section being a wedge is placed at a ramp with a slope angle of 45 degrees. Its mass is 140 kg. The elastic modulus is 72 GPa and Poisson's ratio is 0.33. The friction angle between the rigid slide and the contact surface is 0.6°. In the numerical model, the particle spacing of MPS is set to 2×10^{-2} m, and the time step is set to 1×10^{-4} s. The physical time in actuality is 5 s.

Fig. 3 Schematic sketch of submerged rigid landslide model

Displacement time histories of rigid slide in the vertical direction is shown in Fig. 4. In the initial stage, the numerical results obtained by ISPH (Yeylaghi et al., 2017) are in good agreement with experimental results. However, in the later stage, the velocity of rigid slide observed in simulation increases and the displacement is significantly higher than that in experimental studies. The numerical results of SPH-DDA (Wang et al., 2016) are significantly lower than experimental results in the initial stage. In contrast, the computational results obtained by MPS-DEM are much closer to the experimental data results in general. Additionally, it can be seen that the curve obtained by MPS-DEM is smoother, indicating that under severe disturbances, the fluid pressure and wall friction obtained by the MPS-DEM method are more accurate and stable. In summary, the MPS-DEM coupling method can accurately predict the motion process of rigid slide under fluid action.

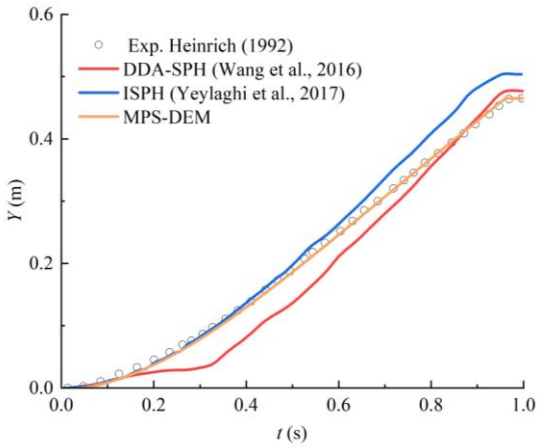

Fig. 4 Displacement time histories of rigid slide in the vertical direction - submerged rigid landslide

Fig. 5 shows the shapes of free surface at t = 0.5 s and t = 1.0 s. Due to the narrow width of the water tank, the waves induced by the landslide do not exhibit significant three-dimensional effects. Therefore, both 2-D and 3-D results obtained by the MPS-DEM coupling method are in good agreement with experimental results, which indicates that the MPS-DEM coupling method can accurately simulate the surges caused by landslide.

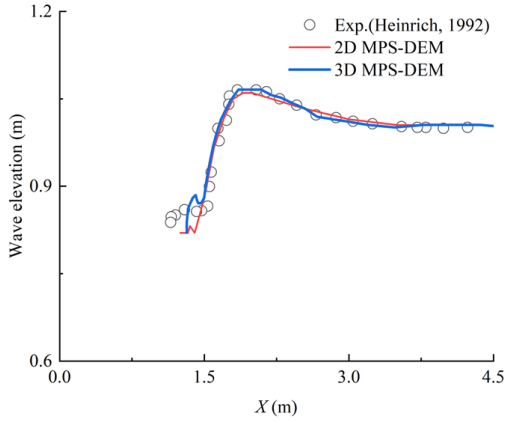

(a1) t = 0.5 s

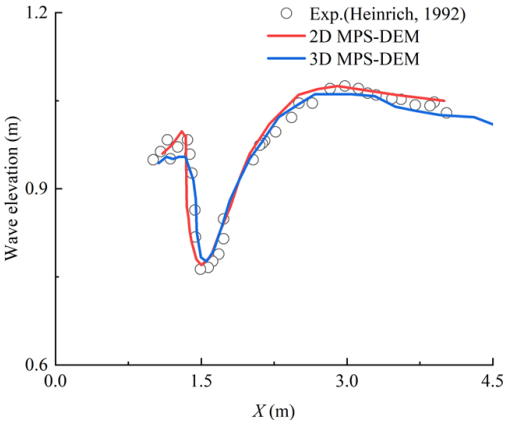

(a2) t = 1.0 s

Fig. 5 The shape of free surface at different instants - submerged rigid landslide

Simulation snapshot obtained by MPS-DEM is shown in Fig. 6. During the process of rigid landslide, the fluid quickly fills the original position of the rigid slide. After the fluid impacts the top of the rigid slide, two flows are generated with opposite velocity directions. One of the flows climbs up along the ramp and its kinetic energy decreases. When it reaches the highest point, it rolls over and generated waves propagate to the right side of the water tank.

Since the wall particles and fluid particles participate in the calculation of the pressure Poisson equation together, the ghost particles near the wall particles obtain the pressure through interpolation. Therefore, the wall particles close to the fluid particles carry the pressure, while the wall particles far away from the fluid particles should not carry the pressure. The types of boundary particles and pressure distribution on the ramp are shown in Figs. 7 and 8. It can be seen that in the numerical results without DBL technology, all boundary particles on the contact face between the rigid slide and the ramp are wall particles, which participate in the solution of the PPE. Therefore, those boundary particles not close to the fluid particles also carry pressure. Besides, the pressure distribution of the flow field around the rigid slide is also affected, which is obviously inconsistent with the actual situation. However, in the numerical results with DBL technology, all boundary particles on the contact face between the rigid slide and ramp are ghost particles, which do not participate in the solution of the PPE. The pressure value of those particles is zero, which is more consistent with the actual physical situation. This indicates that the proposed DBL technology can effectively avoid the incorrect distribution of pressure on the contact surface. Therefore, in subsequent numerical simulations in this paper, DBL technology is employed.

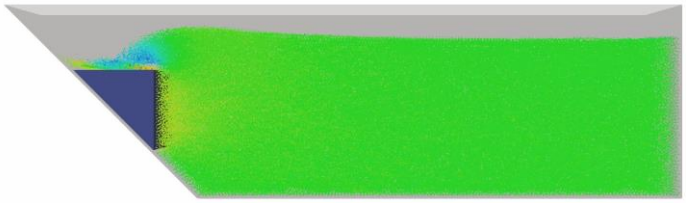

(a1) t = 0.5 s

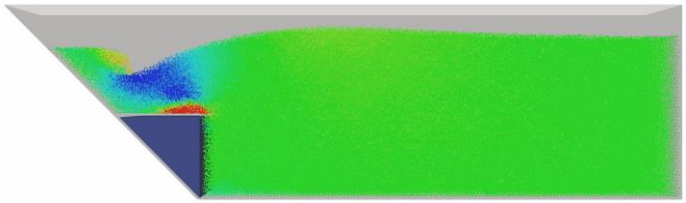

(a2) t = 1.0 s

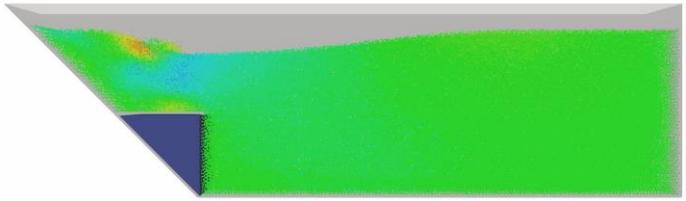

(a3) t = 1.5 s

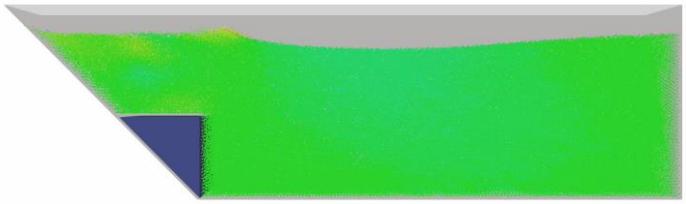

(a3) t = 2.0 s

Fig.6 Simulation snapshot obtained by MPS-DEM - submerged rigid landslide

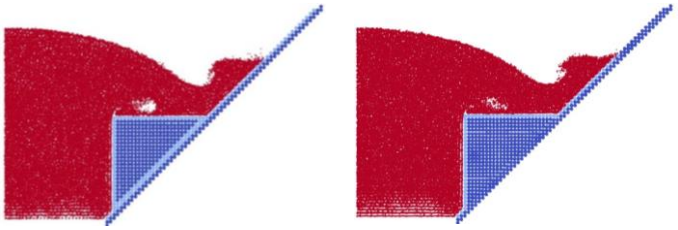

(a) Without DBL technique (b) With DBL technique

Fig.7 Boundary particles' type of the ramp - submerged rigid landslide

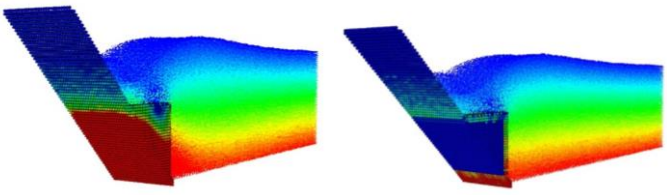

(a) Without DBL technique (b) With DBL technique

Fig.8 Pressure distribution of the ramp - submerged rigid landslide

Subaerial rigid landslide

In this sub-section, the subaerial landslide (Heinrich, 1992) is simulated. the sketch of the numerical model is presented in Fig. 9. The water depth in the tank is 0.4 m. At the initial moment, the slide is placed on the ramp slightly above the water. Other parameters are consistent with that in the simulation of submarine rigid landslide.

Fig. 9 Schematic sketch of subaerial rigid landslide model

Fig.10 shows the displacement time histories of subaerial rigid landslide in vertical direction. It can be seen that the 2-D numerical results obtained by the SPH-DEM coupling method (Tan et al., 2018) are closer to the experimental results in the first half of the landslide process, while the 3-D numerical results simulated by the MPS-DEM coupled method are closer to the experimental results in the second half of the landslide process. Overall, the numerical results of both the MPS-DEM coupled method and the SPH-DEM coupled method are in good agreement with the experimental results. Although the SPH-DEM coupled method can also simulate the contact force between the rigid slide and the ramp, the fluid force exerted on the sliding body is calculated by a semi-empirical formula. In contrast, the hydrodynamic force is calculated through the integration of fluid pressure on the surface of the rigid slide by MPS-DEM couped method, which is more realistic.

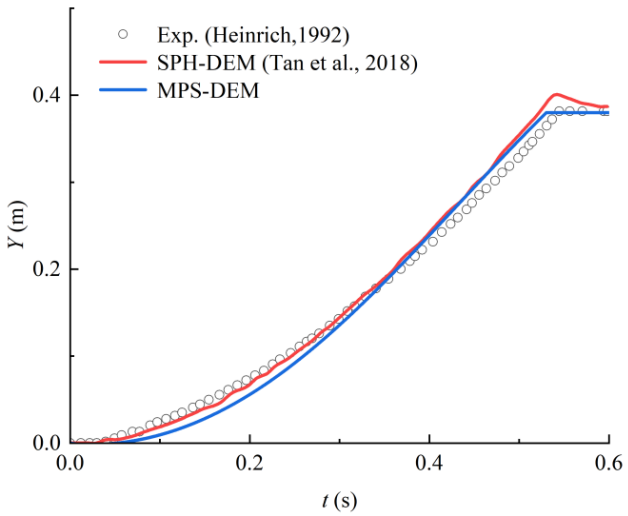

Fig. 10 Displacement time histories of subaerial rigid landslide in vertical direction - subaerial rigid landslide

Fig. 11 shows the shape of free surface at different instants. The two-dimensional and three-dimensional numerical results obtained by MPS-DEM are in good agreement with the experimental results.

Time histories of water surface evolution at x = 4 m is presented in Fig. 12. It can be seen that the curve obtained by the VOF method is significantly smoother than the curve obtained by the MPS-DEM coupled method. This is due to the non-physical pressure oscillation in the simulation by MPS method. Compared to mesh-based methods, the MPS method is more adept at capturing free surfaces. The first and second wave peak values obtained by the MPS method are closer to the experimental values than those obtained by the VOF method. Overall, the MPS-DEM coupling method can accurately simulate the process of subaerial rigid landslide and the propagation of waves.

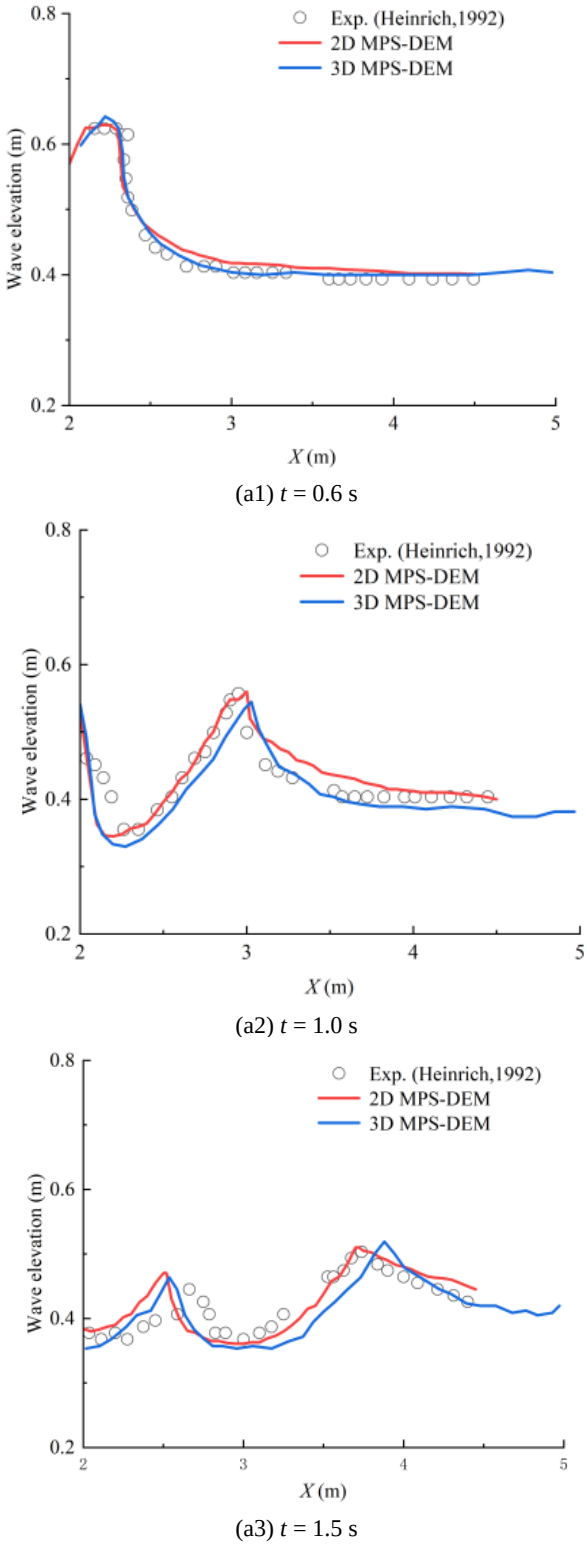

Fig. 11 The shape of free surface at different instants - subaerial rigid landslide

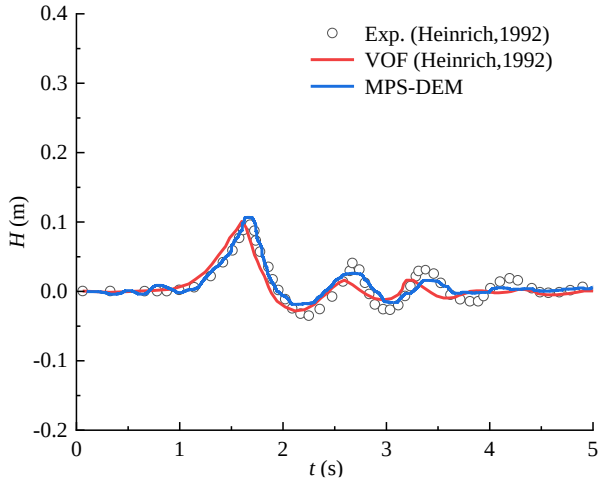

Fig. 12 Time histories of water surface evolution at x = 4 m - subaerial rigid landslide

Fig. 13 shows simulation snapshots obtained by MPS-DEM. Under the action of gravity, the wedge slides down the ramp, giving a forward velocity to the nearby fluid. As the wedge moves, the water level around it rises. At around t = 0.53 s, the wedge suddenly stops due to external forces. Because of the inertia, the fluid detaches from the wedge. At this moment, a significant gap is formed between the wedge and the fluid. At t = 0.75 s, fluid rolls over under the action of gravity, forming the first wave. The fluid velocity is maximum at the wave peak.

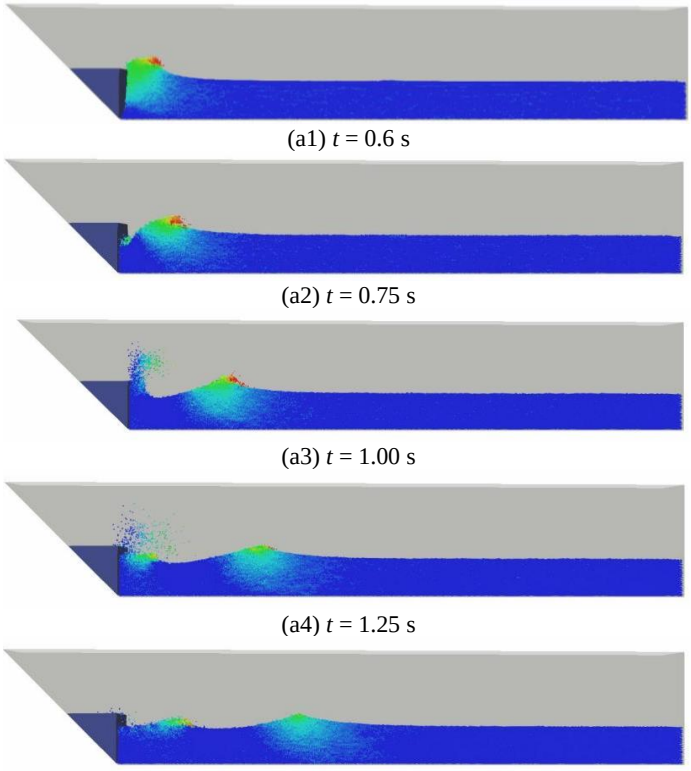

(a1) t = 0.6 s

(a2) t = 0.75 s

(a3) t = 1.00 s

(a4) t = 1.25 s

(a5) t = 1.50 s

Fig. 13 Simulation snapshots obtained by MPS-DEM - subaerial rigid landslide

CONCLUSIONS

In this paper, a 3-D resolved MPS-DEM solver is developed for the simulation of tsunamis induced by rigid landslide. The MPS method is employed to simulate the incompressible fluid flow, while the DEM is used to build the rigid slide-ramp interaction. Besides, a Dynamic Boundary particle Labeling (DBL) technique is proposed, which can significantly reduce the non-physical pressure oscillation. The submarine and subaerial rigid landslides, are conducted by 3-D resolved MPS-DEM coupled method. The numerical result is in good agreement with experimental data, showing the accuracy of the coupled method. In the future, the slide body with more complex shape and multi-bodies slide will be also considered.

ACKNOWLEDGEMENTS

This work is supported by the National Natural Science Foundation of China (52131102), to which the authors are most grateful.

REFERENCES

Amicarelli, A, Albano, R, Mirauda, D, Agate, G, Sole, A, and Guandalini, R (2015). "A Smoothed Particle Hydrodynamics model for 3D solid body transport in free surface flows," *Comput Fluids*, 116: 205-228.

Cundall, P, and Strack, O (1979). "A discrete numerical model for granular assemblies," *Geotechnique*, 1979, 29: 47-65.

Heller, V, Bruggemann, M, Spinneken, J, and Roger, B (2016). "Composite modelling of subaerial landslide–tsunamis in different water body geometries and novel insight into slide and wave kinematics," *Coast Eng*, 109: 20-41.

Heinrich, P (1992). "Nonlinear Water Waves Generated by Submarine and Aerial Landslides," J Waterway Port Coastal Ocean Eng, 118(3): 249-266.

Ji, Z, Fu, L, Hu, X, and Adams, N (2020). "A consistent parallel isotropic unstructured mesh generation method based on multi-phase SPH," *Comput Methods Appl Mech Eng*, 363: 112881.

Khayyer, A, and Gotoh, H (2011). "Enhancement of stability and accuracy of the moving particle semi-implicit method," *J Comput Phy*, 230(8): 3093-3118.

Peng, C, Zhan, L, Wu, W, and Zhang, B (2021). "A fully resolved SPH-DEM method for heterogeneous suspensions with arbitrary particle shape," *Powder Technol*, 387: 509-526.

Qi, Y, Xu, Q, Chen, J, Zhang, J, and Li, J (2022). "Study on solid block landslide generated tsunami using a modified δ-les-SPH model," *Ocean Eng*, 245: 110473.

Tanaka, M, and Masunaga, T (2020). "Stabilization and smoothing of pressure in MPS method by Quasi-Compressibility," *J Comput Phy*, 229(11): 4279-4290.

Tan, H, Xu, Q, and Chen, S (2018). "Subaerial rigid landslide-tsunamis: Insights from a block DEM-SPH model," *Eng Anal Bound Elem*, 95: 297-314.

Wang, W, Chen, G, Zhang, H, Zhou, S, Liu, S, Wu, Y, and Fan, F (2016). "Analysis of landslide-generated impulsive waves using a coupled DDA-SPH method," *Eng Anal Bound Elem*, 64: 267-277.

Xu, W, and Dong, Y (2021). "Simulation and verification of landslide tsunamis using a 3D SPH-DEM coupling method," *Comput Geotech*, 129: 103803.

Yeylaghi, S, Moa, B, Buckham, B, Oshkai, P, Vasquez, J, and Crawford, C (2017). "ISPH modelling of landslide generated waves for rigid and deformable slides in Newtonian and non-Newtonian reservoir fluids," *Adv in Water Resour*, 107: 212-232.

Zhang, G, Chen, J, Qi, Y, Li, J, and Xu, Q (2021). "Numerical simulation of landslide generated impulse waves using a δ+-LES-SPH model," *Adv in Water Resour,* 151: 103890.

Zhang, Y, Wan, D, and Hino, T (2014). "Comparative study of MPS method and level-set method for sloshing flows," *J Hydrodyn,* 26(4): 577-585.

Zhu Y, Zhang C, Yu, Y, and Hu, X (2021). "A CAD-compatible body-fitted particle generator for arbitrarily complex geometry and its application to wave-structure interaction," *J Hydrodyn,* 33(2): 195-206.